Cylindrical Battery Fault Detection under Extreme Fast Charging: A Physics-based Learning Approach

Roya Firoozi, Sara Sattarzadeh, and Satadru Dey

***Abstract*—High power operation in extreme fast charging significantly increases the risk of internal faults in Electric Vehicle batteries which can lead to accelerated battery failure. Early detection of these faults is crucial for battery safety and widespread deployment of fast charging. In this setting, we propose a real-time detection framework for battery voltage and thermal faults. A major challenge in battery fault detection arises from the effect of uncertainties originating from sensor inaccuracies, nominal aging, or unmodelled dynamics. Inspired by physics-based learning, we explore a detection paradigm that combines physics-based models, model-based detection observers, and data-driven learning techniques to address this challenge. Specifically, we construct the detection observers based on an experimentally identified electrochemical-thermal model, and subsequently design the observer tuning parameters following Lyapunov's stability theory. Furthermore, we utilize Gaussian Process Regression technique to learn the model and measurement uncertainties which in turn aid the detection observers in distinguishing faults and uncertainties. Such uncertainty learning essentially helps suppressing their effects, potentially enabling early detection of faults. We perform simulation and experimental case studies on the proposed fault detection scheme verifying the potential of physics-based learning in early detection of battery faults.**

***Index Terms*—Batteries, Extreme Fast Charging, Fault Detection, Physics-based Learning.**

I. Introduction

EXTREME fast charging typically refers to charging a battery to 80% of its capacity within 10 minutes [1]. In extreme fast charging, the goal is to recharge the electric vehicle battery to provide additional 200 miles of range, with high charging power of 350 kW or above [2], [3]. The high power requirement for fast charging significantly increases the risk of internal faults that affect voltage and temperature dynamics. In this research, we address this particular issue of battery safety under fast charging. Existing works on battery fault diagnostics can be broadly classified into two categories: *model-based techniques* and *data-driven techniques*. Examples of such model-based techniques include [4]–[9]. On the other hand, learning-based techniques with meaningful dataset [10] can be useful in circumventing the need for accurate models. For example, data-driven battery diagnostic approaches are presented in [11]–[15]. A long short-term memory network approach is proposed for parameter prediction [16].

However, there are certain limitations associated with these aforementioned approaches: (i) model-based approaches rely on accurate models identification of which can be a cumbersome process; (ii) most of the proposed model-based approaches utilize phenomenological type models which have limited capabilities to capture physical failure modes; (iii) data-driven approaches require significant amount of data encompassing probable fault scenarios, which may not be available in real-world settings; (iv) data-driven approaches might exhibit limitations on diagnosing unforeseen faults which were not present in training data; (v) finally, most of these approaches do not present a systematic way to distinguish fault from uncertainties, which is a fundamental challenge in any fault diagnosis algorithm design. Specific to battery fault detection, the main challenge arises from effect of other (non-faulty) phenomena that cause voltage and temperature deviation. In case of voltage, these phenomena include voltage sensor noise, drift or bias, effect of unmodelled behavior such as electrolyte dynamics (while using a model-based detection approach), and effect of nominal aging which is generally a slower process than faults. Inaccurate heat generation model, temperature sensor noise, drift or bias, and thermal influence of adjacent cells contribute to similar effects in case of temperature. These phenomena, which can be combined as *uncertainties*, prohibit early detection of smaller voltage and thermal faults. Hence, it is imperative to distinguish the effect of *uncertainties* from faults to enable early detection of smaller faults.

In this work, *departing from the existing model-only and data-only diagnostic approaches, we explore a different diagnostics paradigm that combines physics-based models, model-based detection observers, and data-driven learning techniques.* Although physics-model-based and data-driven techniques have been explored separately in some existing works, their meaningful integration to enable better diagnostics remains unexplored. However, it has been shown that meaningfully combining these techniques can potentially lead to easier design and better performance compared to the separate individual techniques [17], [18].

Accordingly, our approach is inspired by model-based learning framework [17], [18]. Our approach can be summarized as follows: (i) we start with a coarsely identified uncertain physics-based model circumventing the cumbersome process of accurate model identification; (ii) we apply an online data-driven learning technique, namely Gaussian Process Regression [19], to learn the uncertainty functions in real-time

This work was supported by National Science Foundation under Grant No. 1908560 and 2050315. The opinions, findings, and conclusions or recommendations expressed are those of the author(s) and do not necessarily reflect the views of the National Science Foundation.

R. Firoozi is with the Department of Mechanical Engineering, University of Berkeley, CA, USA. (e-mail: royafiroozi@berkeley.edu).

S. Dey and S. Sattarzadeh are with the Department of Mechanical Engineering, The Pennsylvania State University, PA 16802, USA. (e-mail: skd5685@psu.edu, sfs6216@psu.edu).

thereby compensating for the model and measurement uncertainties; and (iii) based on the coarsely identified model and aided by the learned uncertainty functions, we design detection observers following Lyapunov's stability theory to diagnose battery faults.

The main advantages of the proposed approach are the following: (i) it can help overcome the limitations of model-based approaches (i.e. need for accurate model and presence of model uncertainties); and (ii) as opposed to data-driven techniques, it does not need for vast data encompassing all possible fault scenarios. In this context, the main contribution of this work lies in a battery diagnostics framework that meaningfully integrates physical model-based detection observers and data-driven learning. Such framework can potentially enable earlier detection of smaller faults at their nascent stage. Specifically, we utilize reduced order electrochemical-thermal model to capture physical behavior and Gaussian Process Regression to learn uncertainty, which collectively leads to a potentially better battery diagnostics framework.

The rest of the paper is organized as follows. Section II describes the phsyics-based battery models. Section III details the proposed fault detection framework. Section IV presents experimental and simulation results with discussion. Finally, section V concludes the work.

II. Battery Electrochemical-Thermal Model

In this section, we discuss the battery model adopted for this work. Specifically, we focus on electrochemical and thermal dynamics of batteries. We adopt the Single Particle Model (SPM) framework to capture electrochemical dynamics and focus on anode dynamics [20], [21]:

$$\frac{\partial c_a(x,t)}{\partial t} = \frac{D}{x^2}\frac{\partial}{\partial x}\Big(x^2\frac{\partial c_a(x,t)}{\partial x}\Big), \tag{1}$$

$$\frac{\partial c_a(x,t)}{\partial x}\Big|_{x=0} = 0, \quad \frac{\partial c_a(x,t)}{\partial x}\Big|_{x=X} = \frac{-I(t)}{a_a F D A_a L_a}, \tag{2}$$

where x is the radial coordinate of the particle in m, t is the time in s, c_a is the Lithium concentration along the particle radius in mol/m^3, D is the anode diffusion coefficient in m^2/s, X is radius of the particle in m, I is the applied current in A with $I > 0$ indicating discharging, a_a is the anode specific surface area in m^2/m^3 which is computed as $a_a = 3\epsilon_a/X$ where ϵ_a is the active material volume fraction, F is the Faraday's constant in C/mol, A_a is the anode current collector area in m^2, and L_a is the anode thickness in m. In SPM framework, electrodes are approximated as spherical particles. Based on such approximation, (1) describes the solid-phase diffusion of Lithium ions in the anode, governed by the volume-averaged current acting on the on the boundary as given in (2).

The battery terminal voltage can be expressed as [21]:

$$V_{term}(t) = U_c\Big(\alpha_1 c_a(X) + \alpha_2\Big) + U_a\Big(c_a(X)\Big) - R_b I(t) + \frac{RT}{\alpha_c F}\sinh^{-1}\Big(\frac{I(t)}{2a_c A_c L_c i_{0c}}\Big) + \frac{RT}{\alpha_a F}\sinh^{-1}\Big(\frac{I(t)}{2a_a A_a L_a i_{0a}}\Big), \tag{3}$$

where V_{term} is the terminal voltage in V; $U_c(.)$ and $U_a(.)$ are the open circuit potential maps of cathode and anode, respectively; $\alpha_1 = -(\epsilon_a A_a L_a)/(\epsilon_c A_c L_c)$ and $\alpha_2 = m_{Li}/(\epsilon_c A_c L_c)$ with m_{Li} being total moles of Lithium in the cell; R is the universal gas constant in J/mol-K, T is the average cell temperature in K, α_c and α_a are unitless charge transfer coefficients of cathode and anode, respectively; a_c in m^2/m^3, A_c in m^2, and L_c in m are the specific area, current collector area, and thickness of the cathode, respectively; i_{0c} and i_{0a} are the exchange current densities of cathode and anode in A/m^2, respectively; R_b is the internal resistance of the cell in Ω. In (3), the first two terms represent the thermodynamic potential of the electrodes, the third term captures the effect of internal Ohmic resistances, and the last two terms represent the electric overpotential of the electrodes.

We adopt the following thermal model [22]:

$$\rho C_p\frac{\partial T(y,t)}{\partial t} = k\frac{\partial^2 T(y,t)}{\partial y^2} + k\frac{1}{y}\frac{\partial T(y,t)}{\partial y} + \frac{\dot{Q}(t)}{V_b}, \tag{4}$$

$$\frac{\partial T(y,t)}{\partial y}\Big|_{y=0} = 0, \quad \frac{\partial T(y,t)}{\partial y}\Big|_{y=Y} = -\frac{h}{k}(T(Y) - T_\infty), \tag{5}$$

where t is the time in s, y is the radial coordinate of the cell in m, Y is the cell radius in m, ρ is the cell density in kg/m^3, C_p is the specific heat in J/kg-K, k is the thermal conductivity in W/m-K, h is the convection coefficient in W/m^2-K, T_∞ is the cooling/ambient temperature, V_b is the cell volume in m^3, and $\dot{Q}$ is the heat generation term computed by [22]

$$\dot{Q}(t) = I(t)\Big\{U_c\Big(\alpha_1 c_a(X) + \alpha_2\Big) + U_a\Big(c_a(X)\Big) - V_{term}(t)\Big\}. \tag{6}$$

The model (4) is derived using energy balance principle and captures the spatio-temporal temperature dynamics along the cell radius in a cylindrical coordinate setting [22]. In (5), the first boundary condition represents the zero temperature gradient in the center whereas the second boundary condition captures the convective heat transfer with the environment. The heat generation model (6) captures the irreversible heat due to electrode polarization [23]. In this work, we have ignored the reversible heat generation effect in (6) to keep the heat generation model simple enough for identification and real-time computation purposes. Typically, the reversible heat model requires additional parameter information (e.g. entropic coefficients) which again leads to cumbersome parameter identification. The effect of such reversible heat is later captured by the uncertainties in thermal model.

Both the nominal electrochemical and thermal models are in Partial Differential Equation (PDE) form. We convert these PDEs to a set of Ordinary Differential Equations (ODEs), and subsequently formulate a state-space model. First, considering the electrochemical PDE model (1)-(2), we discretize the particle radius into $N+1$ nodes with each node's Lithium concentration defined as $c_i = c_a(i\delta_x), i = \{0,1,2,...,N\}$ where $\delta_x = X/N$ is the spatial difference between two adjacent nodes. Next, we follow the method of lines approach

for PDE to ODE conversion leading to the following set of ODEs for each node:

$$\begin{aligned}
\dot{c}_1 &= -2\gamma_1 c_1 + 2\gamma_1 c_2, \\
\dot{c}_i &= (1 - \frac{1}{i})\gamma_1 c_{i-1} - 2\gamma_1 c_i + (1 + \frac{1}{i})\gamma_1 c_{i+1}, \\
\dot{c}_N &= (1 - \frac{1}{N})\gamma_1) c_{N-1} - (1 - \frac{N}{i})\gamma_1 c_N + \beta_1 I, \qquad (7)
\end{aligned}$$

with $c_0 = c_1$ from the boundary condition, $i \in \{2, ..., N-1\}$, $\gamma_1 = D/\delta_x^2$, and $\beta_1 = -(1/a_a F A_a L_a \delta_x)(1 + 1/N)$. In a similar manner, we can discretize the thermal PDE equation (4)-(5) with the nodes $T_j = T(j\delta_y), j = \{0, 1, 2, ..., M\}$ where $\delta_y = Y/M$ and arrive at the following set of ODEs:

$$\begin{aligned}
\dot{T}_1 &= -1.5\gamma_2 T_1 + 1.5\gamma_2 T_2 + \dot{Q}/V_b, \\
\dot{T}_j &= (1 - \frac{1}{2i})\gamma_2 c_{j-1} - 2\gamma_2 T_i + (1 + \frac{1}{2i})\gamma_2 T_{i+1} + \dot{Q}/V_b, \\
\dot{T}_M &= (1 - \frac{1}{2M})\gamma_2 T_{M-1} - (1 - \frac{M}{i})\gamma_1 T_M + \dot{Q}/V_b + \beta_2 T_\infty, \qquad (8)
\end{aligned}$$

with $T_0 = T_1$ from the boundary condition, $j \in \{2, ..., M-1\}$, $\gamma_2 = k/\delta_y^2$, and $\beta_2 = -2\gamma_2 + \gamma_2(1 + 1/2M)(1 - \delta_y h/k)$.

A. Failure Modes

A fault is defined as an unpermitted deviation of a characteristic feature from its nominal behavior [24]. On the other hand, failures and malfunctions are considered as interruptions in a system's functionality that are of permanent and intermittent nature, respectively [24]. Faults can occur in sensors, actuators, or within the internal system due to physical anomalies. In this work, we focus on internal system faults.

In the extreme fast charging applications, the battery cell goes through higher amount of stress than the normal operating scenarios. Accordingly, the probability of the failure is higher than the nominal operation. Some of the critical failure modes are: active material and Lithium inventory loss, undesirable side reactions, electrode fracture, electrolyte decomposition, Lithium plating, internal and external short circuits, electrode fracture, separator puncture, and abnormal heating. Further details of failure modes can be found in [25]. Specific to fast charging, some potential battery faults include Lithium plating, thermal runaway, and mechanical degradation such as stress-induced cathode cracking and separation of current collector and electrode [1], [26]. In this work, we focus on two types of faults that can potentially lead to permanent failures: (i) *voltage faults* that mainly affect terminal voltage, and (ii) *abnormal heating faults* that mainly affect thermal dynamics. Broadly speaking, voltage faults can originate from two potential sources: (i) electrochemical side reactions such as Lithium plating, Solid Electrolyte Inter-phase (SEI) growth, and electrolyte decomposition; and (ii) electrical anomalies such as current leaks, external and internal short circuits. In terms of temporal characteristics, voltage faults can show two types of behavior: (i) incipient type faults that gradually show up in a longer period, e.g. SEI growth, and (ii) abrupt type faults that posses faster dynamics, e.g. Lithium plating. Some potential sources of thermal faults are unwanted side reactions, separator failure, overcharging, and external shock or puncture [27], [28].

Although we focus on fast charging application in this work, the proposed framework can be applicable to other scenarios such as normal charging or discharging modes with minor modifications. In such other scenarios, the model and the detection observer frameworks will remain the same while the Gaussian Process Regression based learning function should be trained with scenario-specific data.

B. Uncertainties

As we will use the output measurements to design fault indicator signals in our detection scheme, we mainly focus on the uncertainties affecting the system outputs, namely, terminal voltage and surface temperature. From a physical viewpoint, the term ω_V captures the following: (i) effect of internal resistive component due to variation in electrolytic conductivity, (ii) effect of internal resistance rise due to power fade type aging, (iii) effect of electrolytic concentration states on voltage, (iv) change in the parameter m_{Li} due to loss of active material and Lithium inventory, and (v) inaccuracies in voltage sensor. Similarly, the term ω_T captures the following: (i) the effect of non-uniform heat generation and non-uniform thermal conductivity on the surface temperature prediction, (ii) inaccurate knowledge of convection coefficient affecting surface temperature prediction, (iii) thermal conductivity variation due to aging, and (iv) inaccuracies in temperature sensor.

C. State-Space Model with Faults and Uncertainties

We define the state vectors $z_1 = [c_1, c_2, ..., c_N]^T$ and $z_2 = [T_1, T_2, ..., T_M]^T$, the inputs $u_1 = I$ and $u_2 = T_\infty$, and the outputs $y_1 = V_{term}$ and $y_2 = T_M$. Applying Euler's discretization and linearization on (3), we formulate the following discrete-time state space model from (7), (3), (6), and (8):

$$z_{1t+1} = A_1 z_{1t} + B_1 u_{1t}, \qquad (9)$$

$$y_{1t} = C_1 z_{1t} + D_1 u_{1t} + \omega_{Vt} + \Delta_{Vt}, \qquad (10)$$

$$z_{2t+1} = A_2 z_{2t} + f_2(z_1, y_1, u_1) + B_2 u_{2t} + \Delta_{Tt}, \qquad (11)$$

$$y_{2t} = C_2 z_{2t} + \omega_{Tt}, \qquad (12)$$

where the subscript t denotes the time index, $A_1 \in \mathbb{R}^{N\times N}$, $B_1 \in \mathbb{R}^{N\times 1}$, $A_2 \in \mathbb{R}^{M\times M}$, $B_2 \in \mathbb{R}^{M\times 1}$, $C_2 = [0, 0, .., 0, 1] \in \mathbb{R}^{1\times M}$, $C_1 \in \mathbb{R}^{1\times N}$, $D_1 \in \mathbb{R}$, and the nonlinear function $f_2(.)$ is derived from (6). Furthermore, the term ω_V captures the model and measurement uncertainties as well as linearization error in electrochemical dynamics, ω_T captures the thermal model and measurement uncertainties, Δ_V captures the voltage fault, and Δ_T captures the thermal fault.

III. Fault Detection Framework

The proposed fault detection scheme is shown in Fig. 1. The scheme consists of following four subsystems that interact with each other: (i) *Electrochemical Detection Observer* receives the measured signals and in turn produces voltage

residual signal r_V. (ii) *Thermal Detection Observer* receives the measured signals and produces thermal residual signal r_T. (iii) *Learning Algorithm* receives the measured signals and produces estimates of the uncertainties ω_T and ω_V. (iv) *Decision Maker* receives the residual signals and makes a decision whether a fault has occurred. Next, we will discuss the details of these subsystems.

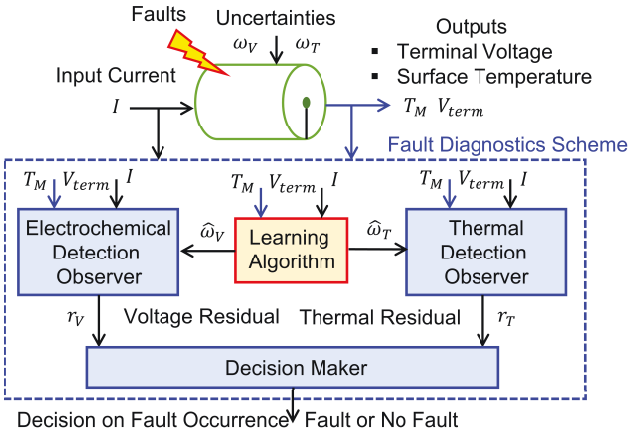

Fig. 1. Fault detection scheme.

A. Gaussian Process Regression based Learning

From fault detection viewpoint, it is a crucial and challenging task to distinguish faults from uncertainties. In this scheme, we utilize Gaussian Process Regression technique to learn the uncertainties in real-time. Gaussian Process Regression technique is a non-parametric kernel-based probabilistic model, which is a well-suited method for long term learning. To update the physics-based models in real-time, we learn and update the uncertainties ω_V and ω_T of the system (10) and (12) using Gaussian Process Regression. Essentially, we follow the Algorithm 1 to implement the learning. Next, we describe the Gaussian Process Regression learning approach outlined in the Algorithm 2.

As explained in the Algorithm 1, in order to use a cycle data as the training set for Gaussian Process Regression, the algorithm 1 first checks if no fault is detected in that cycle, otherwise the cycle data is discarded. So we run the learning algorithm 2 only for no-fault cycles where Δ_{Vt} is zero. Two separate Gaussian Process models are trained to learn voltage ω_V and temperature ω_T uncertainties. To train a Gaussian Process Regression model, the first step is to create a training dataset. We use the previously observed time-series data in the most recent (past) cycle $\mathcal{D}$ as the training set. The dataset contains a matrix of inputs $X \in \mathbb{R}^{N\times 3}$ and a vector of outputs (labels) $Y \in \mathbb{R}^N$, where N denotes the cycle length and 3 denotes the three types of measurement signals. The training dataset is defined as $\mathcal{D} = \{X = \{I_l, V_{term_l}, T_{M_l}\}, Y = \{\omega_l\}\}_{l=1:N}$, where I_l is the input current, V_{term_l} is the measured voltage, and ω_l is the residual between the actual measurements and the predicted values computed by the corresponding model for voltage (10) or temperature (12).

Algorithm 1: Life-time Learning Algorithm

Input: Measured data I, V_{term}, T_M
Output: Uncertainty functions $\hat{\omega}_V$, $\hat{\omega}_T$

1 Initialize $\hat{\omega}_V(.) = 0$, $\hat{\omega}_T(.) = 0$.
2 Based on I, V_{term} and T_M data from *Cycle # 1*, learn the functions $\hat{\omega}_V(.)$ and $\hat{\omega}_T(.)$, using Algorithm 2.
3 **if** *No fault detected in Cycle # M* **then**
  Use I, V_{term} and T_M data from *Cycle # M* to update the functions $\hat{\omega}_V(.)$ and $\hat{\omega}_T(.)$, using Algorithm 2;
else
  Use I, V_{term} and T_M data from the last *Cycle* before *Cycle # M* where no fault is detected;
  Update the functions $\hat{\omega}_V(.)$ and $\hat{\omega}_T(.)$ based on that data, using Algorithm 2;
4 Repeat *Step 3*, till battery End of Life (EOL) is reached.

Algorithm 2: Gaussian Process Learning Algorithm

Input: Training dataset $\mathcal{D}$
Output: Learned uncertainty $\hat{\omega}_{\text{new}}$ with mean μ and covariance σ^2

1 Specify the hyperparameters $(\sigma_p^2, \mathcal{L})$ in (13).
2 Compute the entries of matrix $\mathcal{Q}$ in (14) by evaluating the kernel (13) for the specified hyperparameters.
3 Use (14) to compute (15) and (16).
Return the predicted uncertainty $\hat{\omega}_{\text{new}}$ represented by the mean μ and covariance σ^2 in (15) and (16), respectively.

After creating the dataset, the next step is to train a Gaussian Process Regression model on that data. The algorithm 2 outlines and summarises the steps for training a Gaussian process model. Our goal is to learn a model for the nonlinear function ω_t. Since no prior knowledge is available for ω_t, we choose the prior mean as zero and the covariance between any two data points $\omega(v_l)$ and $\omega(v_q)$ is defined as the squared-exponential kernel [29]

$$k(v_l, v_q) = \sigma_p^2 \exp(-\frac{1}{2}(v_l - v_q)^T \mathcal{L}^{-2}(v_l - v_q)), \qquad (13)$$

where σ_p^2 is the signal variance and the matrix $\mathcal{L}$ is a diagonal matrix and its diagonal elements are length scales that represent the function smoothness parameters. The squared-exponential kernel is widely-used to define the covariance in time-series data and is suitable for modeling smooth functions. Therefore, it is appropriate for our application, since the battery terminal voltage and surface temperature evolve in a sufficiently smooth manner. The unknown hyper-parameters $(\sigma_p^2, \mathcal{L})$ associated with the kernel (13), can either be specified by the user or by maximizing log-likelihood estimation on the training data or by cross-validation on the training data [29]. In this study, we consider the first option, in which the user determines constant hyperparameters by tuning and without performing optimization.

After specifying the hyperparameters, the prior distribution is defined using (13). Then, the joint probability distribution of the new point of interest (test point) and the past observation data is computed as $\begin{bmatrix} \omega \\ \hat{\omega}_{\text{new}} \end{bmatrix} \sim \mathcal{N}(0, \mathcal{Q})$, where ω is the vector of observed data $\omega = \{\omega(v_1), ..., \omega(v_N)\}$ and $\hat{\omega}_{\text{new}}$ is the function value associated with the new point of interest v_{new}. The vector $\mathbf{0} \in \mathbb{R}^{N+1}$ is the mean and the covariance matrix is given by [29]

$$\mathcal{Q} = \begin{bmatrix} \Sigma_{1:N,1:N} & \Sigma_{1:N,\text{new}} \\ \Sigma_{\text{new},1:N} & \Sigma_{\text{new,new}} \end{bmatrix}, \tag{14}$$

where $\Sigma_{1:N,1:N}$ is defined by kernel (13) and has entries $(\Sigma_{1:N,1:N})_{lq} = k(v_l, v_q)$ for $l, q \in \{1, .., N\}$, $\Sigma_{\text{new},1:N}$ is defined as $[k(v_{\text{new}}, v_1), ..., k(v_{\text{new}}, v_N)]$ and $\Sigma_{\text{new,new}}$ is $k(v_{\text{new}}, v_{\text{new}})$. The predictive posterior distribution on our point of interest is calculated as a multivariate Gaussian conditioned on the past observations is $\hat{\omega}_{\text{new}}|\mathcal{D} \sim \mathcal{N}(\mu(\omega_{\text{new}}), \sigma^2(\omega_{\text{new}}))$ [29] with mean μ and covariance σ^2 defined as

$$\mu(\omega_{\text{new}}) = (\Sigma_{\text{new},1:N})(\Sigma_{1:N,1:N})^{-1}\omega \tag{15}$$

$$\sigma^2(\omega_{\text{new}}) = \Sigma_{\text{new,new}} - (\Sigma_{\text{new},1:N})(\Sigma_{1:N,1:N})^{-1}(\Sigma_{1:N,\text{new}}). \tag{16}$$

Note that the Gaussian Process described above is presented in general form. However, to learn voltage and temperature uncertainties we use slightly different Gaussian Processes. To estimate the voltage uncertainty $\hat{\omega}_V$, the training dataset is $\mathcal{D}_V = \{I_l, V_{term_l}, \omega_{Vl}\}_{l=1:\,N}$, where ω_{Vl} is computed as $\omega_{Vl} = V_{term_l} - (C_1 z_{1l} + D_1 u_{1l})$ from (10). Also, to estimate the temperature uncertainty, $\hat{\omega}_T$, the training dataset is $\mathcal{D}_T = \{I, V_{term_l}, T_{Ml}, \omega_{Tl}\}_{l=1:\,N}$ in which T_{Ml} is the measured surface temperature data and ω_{Tl} is computed as $\omega_{Tl} = T_{Ml} - C_2 z_{2l}$ from (12).

Remark 1. As mentioned in Algorithm 1, the uncertainty models $\hat{\omega}_V(.)$ and $\hat{\omega}_T(.)$ are learned and periodically updated online as the battery cycles. Moreover, these uncertainty models capture a small subset of the physical modes as compared to the entire battery model, as clarified in Section II.B. Hence, the uncertainty models require lesser amount of data to be trained. Furthermore, there is no assumption on the uncertainty model structure and operating scenarios. Therefore, such learning framework can be applied to any operating conditions and the algorithm will adapt to the same. Compared to the other learning approaches, Gaussian Process Regression is suitable for online learning in our application. Since the battery uncertainty model can potentially exhibit nonlinearities, linear regression approaches are not well-suited for our application. On the other hand, the nonlinear regression methods such as nonlinear least square technique require solving a nonlinear optimization iteratively which leads to slow convergence rates and therefore not applicable for online learning. Compared to nonlinear least squares, Gaussian Process does not require iterative optimization and the estimates are simply computed based on (15). Additionally, compared to the Extended Kalman Filtering (EKF), Gaussian process does not need linearization step. Furthermore, another advantage of Gaussian Process is that it gives a reliable estimate of its own uncertainty presented in (16). This uncertainty can be used in non-deterministic settings for observer design as well.

B. Design of Detection Observers

Based on the electrochemical and thermal models (9)-(10) and (11)-(12), we choose the following structure for the detection observers:

$$\hat{z}_{1t+1} = A_1 \hat{z}_{1t} + B_1 u_{1t} + L_V(y_{1t} - \hat{y}_{1t}), \tag{17}$$

$$\hat{y}_{1t} = C_1 \hat{z}_{1t} + D_1 u_{1t} + \hat{\omega}_{Vt}, \tag{18}$$

$$r_{Vt} = y_{1t} - \hat{y}_{1t}, \tag{19}$$

$$\hat{z}_{2t+1} = A_2 \hat{z}_{2t} + f_2(\hat{z}_1, y_1, u_1) + B_2 u_{2t} + L_T(y_{2t} - \hat{y}_{2t}), \tag{20}$$

$$\hat{y}_{2t} = C_2 \hat{z}_{2t} + \hat{\omega}_{Tt}, \tag{21}$$

$$r_{Tt} = y_{2t} - \hat{y}_{2t}, \tag{22}$$

where $\hat{k}$ is the estimate of k, $L_V \in \mathbb{R}^{N\times 1}$ and $L_T \in \mathbb{R}^{M\times 1}$ are the observer gains to be designed, and $\hat{\omega}_V$ and $\hat{\omega}_T$ are the estimate of the uncertainties provided by the learning algorithm. Subsequently, subtracting (17)-(18) from (9)-(10) and (11)-(12) from (20)-(21), we can write the observers' error dynamics as:

$$\tilde{z}_{1t+1} = (A_1 - L_V C_1)\tilde{z}_{1t} - L_V(\Delta_{V_2 t} + \epsilon_{Vt}), \tag{23}$$

$$r_{Vt} = \tilde{y}_{1t} = C_1 \tilde{z}_{1t} + \Delta_{Vt} + \epsilon_{Vt}, \tag{24}$$

$$\tilde{z}_{2t+1} = (A_2 - L_T C_2)\tilde{z}_{2t} + \tilde{f}_2 + \Delta_{Tt} - L_T \epsilon_{Tt}, \tag{25}$$

$$r_{Tt} = \tilde{y}_{2t} = C_2 \tilde{z}_{2t} + \epsilon_{Tt}, \tag{26}$$

where $\tilde{k} = k - \hat{k}$ is the estimation error, $\tilde{f}_2 = f_2(z_1, y_1, u_1) - f_2(\hat{z}_1, y_1, u_1)$, ϵ_V and ϵ_T represent the error in learned uncertainties.

Next, we present the following proposition that illustrates the convergence properties of the error dynamics and residual signals as well as design conditions for the observer gains L_V and L_T.

Proposition 1. *Considering the estimation error dynamics* (23)-(26)*, the following are true:*

1) *in the presence of no fault and no learning error, i.e.* $\Delta_V = 0, \Delta_T = 0, \epsilon_V = 0, \epsilon_T = 0$*, the estimation errors* $\tilde{z}_1$ *and* $\tilde{z}_2$*, and the residual signals* r_V *and* r_T *will asymptotically converge to zero starting from any non-zero initial condition;*
2) *in the presence of only learning error and no fault, i.e.* $\Delta_V = 0, \Delta_T = 0, \epsilon_V \neq 0, \epsilon_T \neq 0$*, the estimation errors* $\tilde{z}_1$ *and* $\tilde{z}_2$*, and the residual signals* r_V *and* r_T *will remain uniformly bounded;*
3) *in the presence of both learning error and fault, i.e.* $\Delta_V \neq 0, \Delta_T \neq 0, \epsilon_V \neq 0, \epsilon_T \neq 0$*, the estimation errors* $\tilde{z}_1$ *and* $\tilde{z}_2$*, and the residual signals* r_V *and* r_T *will remain uniformly bounded;*

if there exist symmetric positive definite matrices P_1 *and* P_2 *such that the following conditions are satisfied:*

$$-\underline{\lambda}_Q + \Gamma x_1 < 0, \quad -\underline{\lambda}_Z + \vartheta x_2 < 0. \tag{27}$$

where Γ *and* ϑ *are arbitrary positive numbers,* $x_1 = \left\|(A_1 - L_V C_1)^T P_1\right\|$, $x_2 = \left\|(A_2 - L_T C_2)^T P_2\right\|$, $\underline{\lambda}_Q$ *and* $\underline{\lambda}_Z$

are the minimum eigen values of $[P_1-(A_1-L_VC_1)^TP_1(A_1-L_VC_1)]$ *and* $[P_2-(A_2-L_TC_2)^TP_2(A_2-L_TC_2)]$, *respectively.*

Proof. See Appendix. □

C. Design of Decision Maker

The decision maker decides whether a fault has occurred based on the following detection logic:

$$r_i \leq \delta_i \implies \text{no fault}, r_i > \delta_i \implies \text{fault occurrence}, \quad (28)$$

where $i \in \{V, T\}$ and δ_i are the thresholds. Note that even with learning algorithm there is always a possibility that the residual signals will be non-zero even under no fault conditions. The thresholds δ_i deal with this issue and provide robustness to such errors. Next, the following steps are performed for threshold selection.

Step 1: We run the learning-based detection observers under different no-fault operating conditions. Typically, such operating scenarios are generated using Monte-Carlo type of simulation studies or experimental studies. As we focus on fast charging scenarios in this work, we run the observers under experimental fast charging cycles. Such runs produce residual signal data r_i under no-fault but uncertain conditions. Referring to (9)-(12) and (17)-(26), these conditions mean $\omega_i \neq 0$ and $\Delta_i = 0$. Furthermore, considering (24) and (26), the amplitudes of r_i depend on the amplitudes of the learning error ϵ_i, (i.e. $r_i(\epsilon_i)$).

Step 2: Next, we find the maximum absolute amplitude of the residual data r_i collected in *Step 1* and set that value as the threshold δ_i, that is $\delta_i = \max|r_i|$. Effectively, such threshold is related to the maximum learning error in the learning-based detection observers. In other words, the threshold approximately equals to the upper bound of the residuals under uncertain but no-fault conditions, assuming the data r_i comprehensively capture no-fault operating scenarios.

Remark 2. The robustness of the proposed approach is enabled by following: (i) The use of uncertainty learning function reduces the effect of model uncertainties; (ii) output feedback-based diagnostic observers further suppress the uncertainties arising from learning errors; and (iii) finally, the use of thresholds allows us to suppress the combined effect of uncertainties to certain extent.

IV. Results and Discussion

In the following subsections, we discuss the results of the proposed fault detection scheme. All experiments are conducted on Arbin battery testing system. First, we identify the nominal electrochemical-thermal model for a commercial 18650 Lithium-ion battery cell based on experimental current, terminal voltage, and surface temperature data. The cell has the following characteristics: Graphite anode and NMC cathode, 3 Ah nominal capacity, terminal voltage range 4.2-2.5 V, and maximum fast charge current 4 A. Essentially, we have solved the following optimization problem to identify the cell parameters: $\min_{\theta} rms\{X_e - X_m(\theta)\}$ with subject to (3), (7), (6), and (8) where X_e and X_m denote experimental and model voltage and temperature data, respectively, and $\theta = \{D, A_a, A_c, R_b, m_{Li}, \epsilon_a, \epsilon_c, h, C_p, k\}$ is the parameter vector identified as D=1.022 $\times$ 10^{-14} m^2/s, A_a=0.09 m^2, A_c=0.048 m^2,ϵ_a=0.8, ϵ_c=0.6516, R_b=0.006 Ω, m_{Li}=0.1796 $moles$, h=16.78 $W/(m^2-K)$, C_p=907 $J/(kg-K)$, k=1.79 $W/(m-K)$. We have used this identified model for the subsequent case studies. The learning algorithm is also applied to learn the uncertainty models. In this particular case, we have used battery data from cycle # 1 through cycle # 40 under constant current constant voltage (CCCV) charging to train the uncertainty models. A comparison of the model and experimental data under CCCV charging is shown in Fig. 2.

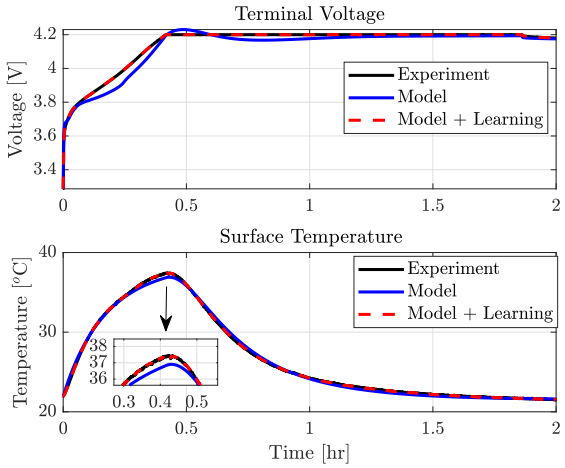

Fig. 2. Comparison of model output and experimental data under constant current constant voltage (CCCV) charging scenario. For model only case, the RMS errors are 27.4 mV and 0.3 ^oC whereas model along with learning have RMS errors of 0.56 mV and 0.012 ^oC.

A. Voltage Fault Detection

In this section, we test the performance of the proposed fault diagnosis scheme under voltage fault. As mentioned before, a voltage fault can be caused by different internal anomalies. In this study, we mainly focus on abrupt type voltage fault caused by Lithium plating which is a highly probably fault mode under fast charging [1], [26]. However, the proposed approach is applicable to other type of voltage faults as well. To emulate the fault, we considered the fast charge current scenario with 4 A charging current, as per the battery cell datasheet. We have not chosen a charging current higher than the prescribed fast charge conditions due to safety reasons in our laboratory experiment setting. Although we have chosen such fast charge conditions for this experiment, the proposed approach is still valid for higher values of charging current. We have modified the nominal terminal voltage by adding a faulty voltage component mimicking the voltage data under Lithium plating presented in [30]. As shown in [30], the voltage plateau in lower State-of-Charge region exhibits a *overshoot* type behavior under Lithium plating during high current charging, which is not present in the absence of plating. Experimental voltage data during high current charging and corresponding prediction of Lithium plating is shown in Fig. 1 of [30]. We incorporate similar *overshoot* type behavior in our voltage fault injection. The faulty voltage component is modelled as:

$a_1 e^{-0.5(x_1-\mu)} + a_2 \sin(x_2)$ where $x_1 \in [-\pi, \pi], x_2 \in [\frac{\pi}{3}, \pi]$ where a_1 and a_2 represent the fault magnitude. Subsequently, such faulty voltage data was fed to the electrochemical detection observer to test its performance. The threshold has been designed to be $\delta_V = 0.01$ V following the process mentioned in Section III.C. We have tested four fault cases that capture various magnitudes: Fault case 1: $a_1 = 0.003$ and $a_2 = 0.0075$, Fault case 2: $a_1 = 0.0048$ and $a_2 = 0.0120$, Fault case 3: $a_1 = 0.009$ and $a_2 = 0.0225$. The responses of the terminal voltage (V_t) and voltage residual (r_V) under these faults are shown in Fig. 3. It is observed that all the fault cases are detected as the residuals crossed the threshold in 89, 70 and 49 seconds, respectively. However, Fault case 1 found to be the minimum fault size that can be detected. This illustrates the effectiveness of the proposed scheme in detecting voltage faults.

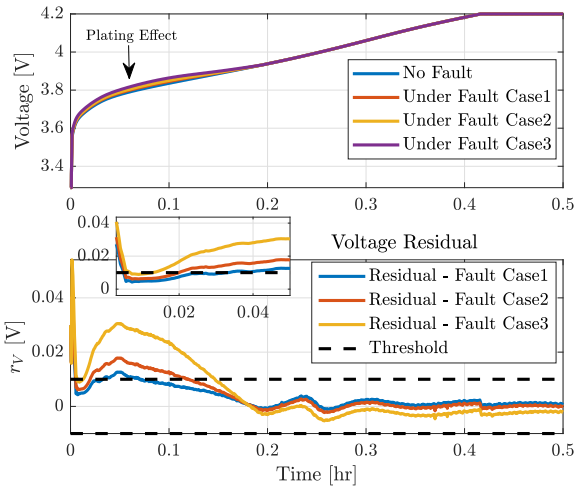

Fig. 3. Residual responses under voltage faults.

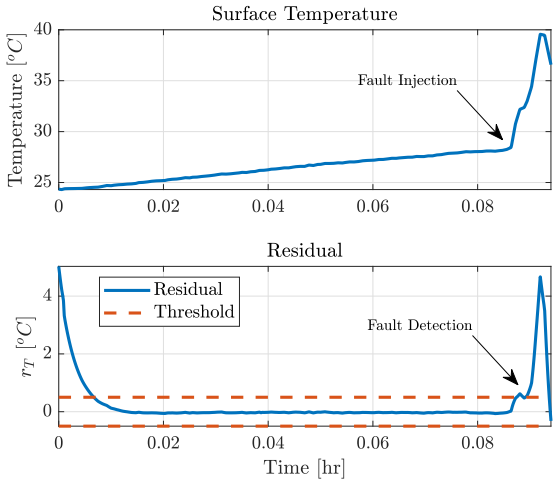

Fig. 4. Residual response under thermal fault.

B. Thermal Fault Detection

Here we discuss an experimental case study under thermal fault. To emulate the thermal fault scenario in experimental setting, we have used an external heater to inject heat on the surface of the battery cell. As it is difficult to induce an internal thermal fault in a controlled and safe manner, we have used such external heater to emulate the thermal fault scenario. Although from a physical experiment viewpoint this fault is emulated via external means, it effectively shows up in the last state equation (last equation of (8)) as an additive fault. Such fault model is also consistent with the Δ_T term in (11), where the vector Δ_T has all zero elements except for the last element in this particular case. Hence, from the fault model point of view, the externally emulated fault is consistent with the modelling assumption. We have also used similar fault emulation approach in our previous work [4].

In response to such injected heat, battery temperature increased until the external heat has been turned off. The surface temperature response under this experiment is shown in the top plot of Fig. 4. Until 311 s, the temperature was increasing under natural conditions as the cell was being charged with a constant current. At 311 s, a thermal fault was injected via an external heater which was taken off around 331 s. In response to this fault, the temperature started increasing abnormally until 331 s and then started to come down. This temperature data is fed to the proposed fault detection algorithm in order to verify its performance. The threshold has been designed to be $\delta_T = 0.5^o$C following the process mentioned in Section III.C. The residual evolution is shown in the bottom plot of Fig. 4. The residual signal r_T started from a non-zero initial condition due to initial condition error. After a while, r_T converged close to zero and stayed within the threshold δ_T. Subsequently, in response to the injected thermal fault, the residual signal r_T crossed the threshold at 315 thereby detecting the fault within 4 seconds of its occurrence. Furthermore, the residual converged back within the threshold when the fault disappeared around 331 s.

C. Minimum Detectable Thermal Fault

Generally speaking, fault size needs to exceed a certain magnitude for the diagnostics algorithms to be able to detect it, owing to various practical limitations. This essentially translates to a minimum detectable non-zero fault. In our study, such limitation arises from the threshold value. In this context, here we explore the minimum size of the thermal fault detectable by the proposed scheme. We have simulated three thermal faults of decreasing magnitudes. Case 1: magnitude 310 W, Case 2: magnitude 220 W, Case 3: magnitude 100 W. The surface temperature response under these three faults are shown in the top plot of Fig. 5. Similar to the previous case study, the temperature was increasing under natural conditions as the cell was being charged with a constant current until 311 s. Subsequently, faults were injected at 311 s leading to abnormal increase in temperature. These data were fed to the algorithm. The residual responses under these faults are shown in the bottom plot of Fig. 5. The residual signal r_T started from a non-zero initial condition and subsequently converged close to zero and stayed within the threshold δ_T. In response

to the thermal faults, r_T showed some deviation. However, r_T crossed the threshold only for Cases 1 and 2 thereby detecting these faults. Case 3 fault was not detected as r_T did not deviate enough. Hence, we observed that: (i) the Case 1 and Case 2 faults were detected within 4 seconds, and (ii) the minimum detectable fault size is around 200 W which is slightly less than the fault in Case 2.

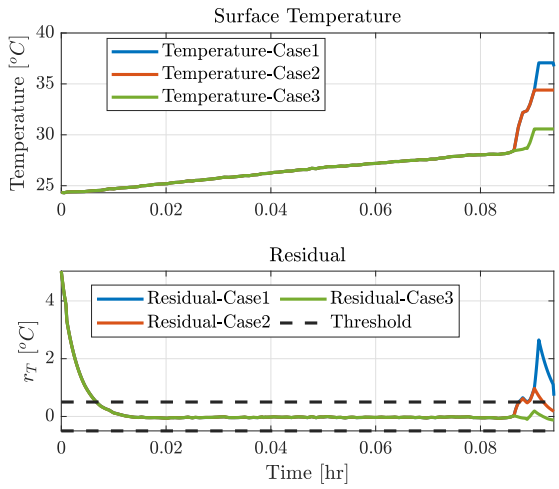

Fig. 5. Thermal fault detection performance.

D. Performance Comparison of Model-only and Model-and-Learning Approaches

In this section, we compare the performance of the scheme with and without learning. In the first comparative study, we consider two cases under voltage fault (Fault case 3 in Section IV.A): (i) *Case 1*, where the learning algorithm is used in conjunction with the detection observer, and (ii) *Case 2*, where only the detection observer has been used without any learning algorithm. The detection observer in *Case 2* has been designed following standard eigen-value placement based approach. For both of these cases, there is a *decision maker* which uses the same threshold based approach mentioned in Section III.C. It should be noted that the threshold for *Case 2* (0.075 V) is higher than that of *Case 1* (0.01 V). This is expected since in *Case 2* the residual signal is corrupted with significantly more amount of uncertainties as there is no learning algorithm. On the other hand, the residual signal in *Case 1* is much less affected by uncertainties due to learning. The residual responses under no fault condition and faulty condition are shown in Fig. 6. We can see that the residual crosses the threshold after the terminal voltage started showing faulty behavior for *Case 1*. However, the residual signal does not cross the threshold for *Case 2*. This shows that the use of learning algorithm can potentially detect smaller faults which would be undetected by without learning based approaches. Note that the gain in performance comes at the cost of training and implementation requirement of the learning algorithm. Such implementation would require additional tuning of the hyper-parameters and computational power to process the learning.

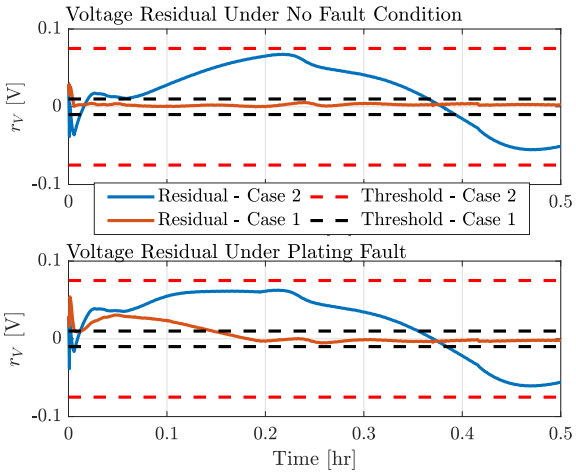

Fig. 6. Comparison of with and without learning based detection approaches under Lithium plating fault.

E. Performance under Uncertainties

In this section, the robustness of proposed scheme is studied under parametric uncertainties. Specifically, we illustrate how parametric uncertainties can lead to false alarms. We study two cases: (i) performance of the electrochemical observer with uncertainty in the parameter a_a; (ii) performance of the temperature observer with uncertainty in the parameter R_b. The results are shown in Fig. 7. We observed that the performance degrades in terms of false alarm beyond 10% uncertainty in a_a and 20% uncertainty in R_b. The parameters a_a and R_b also capture battery aging as R_b increases and a_a decreases with the cycling process. Hence, these results are effectively run under different State-of-Health condition of the battery cell. This illustrates that the proposed approach is also adaptive to battery aging to a certain extent.

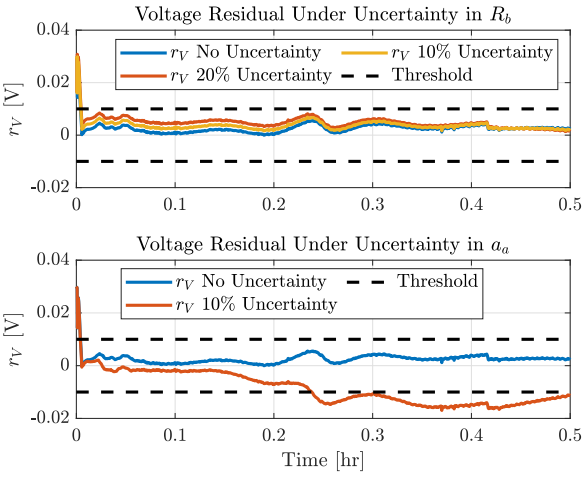

Fig. 7. Voltage residuals under uncertainties in a_a and R_b.

In summary, this section presents a combination of simulation and experimental studies to illustrate the effectiveness of the proposed approach. Section IV.A discusses the performance of the proposed approach under voltage fault

by illustrating a case of Lithium plating faults. It has been found that these fault cases were detected within 89 seconds. A representative minimum detectable fault size is also presented under plating fault cases. Section IV.B discusses the performance of the proposed approach under thermal faults using experimental faulty data where the fault is detected in 4 seconds. Section IV.C presents a representative minimum detectable thermal fault size of 200 W. Section IV.D illustrates the advantages of combining model- and data-based methods over model-only methods by showing that a representative small fault detected by the proposed approach goes undetected by a model-only method. This highlights the potential of the proposed approach for better diagnostics. Finally, Section IV.E studies the robustness of the proposed approach under parametric uncertainties where it is found that the performance degrades beyond 10% uncertainty in a_a and 20% uncertainty in R_b.

V. Conclusion

In this paper, we have studied a battery fault detection paradigm combining physics-based models with detection observer technique and Gaussian Process regression to detect voltage and thermal faults. Based on an experimentally identified electrochemical-thermal model, we have performed the following case studies: simulation study on voltage fault detection and experimental study on thermal fault detection. These case studies have shown the effectiveness of the proposed detection approach for battery fault detection. We plan to study future extensions including fault estimation, more comprehensive physics-based models, and battery packs. Furthermore, we also plan to improve threshold design approach utilizing comprehensive battery data under faulty and non-faulty conditions. Finally, rigorous testing of the proposed approach using comprehensive real-world dataset (for example, the datasets in [10] and [31]) will be considered as future extension of this study.

Appendix
Proof of Proposition 1

First, we consider the following Lyapunov function candidate to analyze electrochemical detection observer error dynamics $W_{1t} = \tilde{z}_{1t}^T P_1 \tilde{z}_{1t}$ where P_1 is a positive definite symmetric matrix. The first order difference in the Lyapunov function is given by:

$$\begin{aligned}\Delta W_1 =&\tilde{z}_{1t}^T[(A_1 - L_V C_1)^T P_1 (A_1 - L_V C_1) - P_1]\tilde{z}_{1t} \\ &+ 2\tilde{z}_{1t}^T (A_1 - L_V C_1)^T P_1 \eta_{1t} + \eta_{1t}^T P_1 \eta_{1t}. \quad (29)\end{aligned}$$

where $\eta_1 = -L_V(\Delta_V + \epsilon_V)$. Next, we prove the three statements of Proposition 1 separately.

Proof of Statement (1): In the presence of no fault and no learning error, i.e. $\Delta_V = 0, \epsilon_V = 0$, we can write (29) as

$$\begin{aligned}&\Delta W_1 = \tilde{z}_{1t}^T[(A_1 - L_V C_1)^T P_1 (A_1 - L_V C_1) - P_1]\tilde{z}_{1t}, \\ &\implies \Delta W_1 \leq -\underline{\lambda}_Q \left\|\tilde{z}_{1t}\right\|^2. \quad (30)\end{aligned}$$

If first equation of (27) is satisfied, we have $-\underline{\lambda}_Q < 0$ as $x_1 > 0$ and $\Gamma > 0$. Consequently, we have $\Delta W_1 < 0$. Hence, the estimation error $\tilde{z}_1$ and the residual signal r_V will asymptotically converge to zero starting from a non-zero initial condition. This proves that the proposed diagnostic scheme is robust to unknown initial conditions.

Proof of Statement (2): In the presence of learning error and no fault, i.e. $\Delta_V = 0, \epsilon_V \neq 0$, we can write (29) as

$$\begin{aligned}\Delta W_1 =&\tilde{z}_{1t}^T[(A_1 - L_V C_1)^T P_1 (A_1 - L_V C_1) - P_1]\tilde{z}_{1t} \\ &+ 2\tilde{z}_{1t}^T (A_1 - L_V C_1)^T P_1 \eta^*{}_t + \eta^*{}_t^T P_1 \eta^*{}_t. \quad (31)\end{aligned}$$

where $\eta^* = -L_V \epsilon_V$. Considering Holder's inequality and the inequality $2ab \leq \Gamma a^2 + \frac{1}{\Gamma} b^2$ with $a, b, \Gamma > 0$, we can further re-write (31) as

$$\Delta W_1 \leq (-\underline{\lambda}_Q + \Gamma x_1) \left\|\tilde{z}_{1t}\right\|^2 + (\overline{\lambda}_P + \frac{x_1}{\Gamma}) \left\|\eta^*{}_t\right\|^2, \quad (32)$$

where Γ is an arbitrary positive number, $x_1 = \left\|(A_1 - L_V C_1)^T P_1\right\|$, $\underline{\lambda}_Q$ is the minimum eigen value of $[P_1 - (A_1 - L_V C_1)^T P_1 (A_1 - L_V C_1)]$, $\overline{\lambda}_P$ is the maximum eigen value of P_1. If first equation of (27) is satisfied, then we have $-\underline{\lambda}_Q + \Gamma x_1 < 0$. Under this scenario, we can only guarantee $\Delta W_1 < 0$ under the condition $\left\|\tilde{z}_{1t}\right\|^2 > -\frac{(\overline{\lambda}_P + \frac{x_1}{\Gamma})}{(-\underline{\lambda}_Q + \Gamma x_1)} \left\|\eta^*{}_t\right\|^2$. Hence, we can conclude that the estimation error $\tilde{z}_1$ and the residual signal r_V will be uniformly bounded and converge within a ball of radius. This proves that the proposed diagnostic scheme is robust to uncertainties originating from learning errors.

Proof of Statement (3): In the presence of learning error and fault, i.e. $\Delta_V \neq 0, \epsilon_V \neq 0$, we can use (29) as is, and prove uniform stability under both fault and learning errors following the steps in the proof of statement (2). This proves that the proposed diagnostic scheme will produce stable residuals under faults and uncertainties originating from learning errors.

Following similar steps, we can prove the convergence for the thermal detection observer.

References

[1] S. Ahmed, I. Bloom, A. N. Jansen, T. Tanim, E. J. Dufek, A. Pesaran, A. Burnham, R. B. Carlson, F. Dias, K. Hardy *et al.*, "Enabling fast charging–A battery technology gap assessment," *Journal of Power Sources*, vol. 367, pp. 250–262, 2017.

[2] X. Chen, Z. Li, H. Dong, Z. Hu, and C. C. Mi, "Enabling extreme fast charging technology for electric vehicles," *IEEE Transactions on Intelligent Transportation Systems*, vol. 22, no. 1, pp. 466–470, 2020.

[3] C. J. Michelbacher, S. Ahmed, I. Bloom, A. Burnham, B. Carlson, F. Dias, E. J. Dufek, A. N. Jansen, M. Keyser, D. Howell *et al.*, "Enabling Fast Charging: A Technology Gap Assessment," Idaho National Lab.(INL), Idaho Falls, ID (United States), Tech. Rep., 2017.

[4] S. Dey, H. E. Perez, and S. J. Moura, "Model-based battery thermal fault diagnostics: Algorithms, analysis, and experiments," *IEEE Transactions on Control Systems Technology*, vol. 27, no. 2, pp. 576–587, 2017.

[5] S. Dey and B. Ayalew, "A diagnostic scheme for detection, isolation and estimation of electrochemical faults in lithium-ion cells," in *ASME 2015 Dynamic Systems and Control Conference*. American Society of Mechanical Engineers Digital Collection, 2015.

[6] J. Marcicki, S. Onori, and G. Rizzoni, "Nonlinear fault detection and isolation for a lithium-ion battery management system," in *ASME 2010 Dynamic Systems and Control Conference*. American Society of Mechanical Engineers Digital Collection, 2010, pp. 607–614.

[7] J. Wei, G. Dong, and Z. Chen, "Lyapunov-based thermal fault diagnosis of cylindrical lithium-ion batteries," *IEEE Transactions on Industrial Electronics*, 2019.

[8] R. Xiong, R. Yang, Z. Chen, W. Shen, and F. Sun, "Online fault diagnosis of external short circuit for lithium-ion battery pack," *IEEE Transactions on Industrial Electronics*, 2019.

[9] W. Han, L. Zhang, and Y. Han, "Computationally efficient methods for state of charge approximation and performance measure calculation in series-connected battery equalization systems," *Journal of Power Sources*, vol. 286, pp. 145–158, 2015.

[10] X. Tang, K. Liu, K. Li, W. D. Widanage, E. Kendrick, and F. Gao, "Recovering large-scale battery aging dataset with machine learning," *Patterns*, vol. 2, no. 8, p. 100302, 2021.

[11] B. Saha and K. Goebel, "Uncertainty management for diagnostics and prognostics of batteries using bayesian techniques," in *2008 IEEE Aerospace Conference*. IEEE, 2008, pp. 1–8.

[12] Y. Zhao, P. Liu, Z. Wang, L. Zhang, and J. Hong, "Fault and defect diagnosis of battery for electric vehicles based on big data analysis methods," *Applied Energy*, vol. 207, pp. 354–362, 2017.

[13] Y. Zhang, R. Xiong, H. He, and M. G. Pecht, "Long short-term memory recurrent neural network for remaining useful life prediction of lithium-ion batteries," *IEEE Transactions on Vehicular Technology*, vol. 67, no. 7, pp. 5695–5705, 2018.

[14] D. Li, Z. Zhang, P. Liu, Z. Wang, and L. Zhang, "Battery Fault Diagnosis for Electric Vehicles Based on Voltage Abnormality by Combining the Long Short-Term Memory Neural Network and the Equivalent Circuit Model," *IEEE Transactions on Power Electronics*, vol. 36, no. 2, pp. 1303–1315, 2020.

[15] H. Lee, K. Kim, J.-H. Park, G. Bere, J. J. Ochoa, and T. Kim, "Convolutional neural network-based false battery data detection and classification for battery energy storage systems," *IEEE Transactions on Energy Conversion*, 2021.

[16] J. Hong, Z. Wang, W. Chen, and Y. Yao, "Synchronous multi-parameter prediction of battery systems on electric vehicles using long short-term memory networks," *Applied Energy*, vol. 254, p. 113648, 2019.

[17] F. Berkenkamp and A. P. Schoellig, "Safe and robust learning control with gaussian processes," in *2015 European Control Conference (ECC)*. IEEE, 2015, pp. 2496–2501.

[18] B. Recht, "A tour of reinforcement learning: The view from continuous control," *Annual Review of Control, Robotics, and Autonomous Systems*, vol. 2, pp. 253–279, 2019.

[19] C. E. Rasmussen, "Gaussian processes in machine learning," in *Summer School on Machine Learning*. Springer, 2003, pp. 63–71.

[20] S. Santhanagopalan and R. E. White, "Online estimation of the state of charge of a lithium ion cell," *Journal of power sources*, vol. 161, no. 2, pp. 1346–1355, 2006.

[21] S. Dey, B. Ayalew, and P. Pisu, "Nonlinear robust observers for state-of-charge estimation of lithium-ion cells based on a reduced electrochemical model," *IEEE Transactions on Control Systems Technology*, vol. 23, no. 5, pp. 1935–1942, 2015.

[22] S. A. Hallaj, H. Maleki, J. Hong, and J. Selman, "Thermal modeling and design considerations of lithium-ion batteries," *Journal of Power Sources*, vol. 83, no. 1, pp. 1 – 8, 1999.

[23] M. Guo and R. E. White, "Thermal model for lithium ion battery pack with mixed parallel and series configuration," *Journal of the Electrochemical Society*, vol. 158, no. 10, p. A1166, 2011.

[24] R. Isermann, *Fault-diagnosis systems: an introduction from fault detection to fault tolerance*. Springer Science & Business Media, 2005.

[25] X. Hu, K. Zhang, K. Liu, X. Lin, S. Dey, and S. Onori, "Advanced Fault Diagnosis for Lithium-Ion Battery Systems: A Review of Fault Mechanisms, Fault Features, and Diagnosis Procedures," *IEEE Industrial Electronics Magazine*, vol. 14, no. 3, pp. 65–91, 2020.

[26] A. Tomaszewska, Z. Chu, X. Feng, S. O'Kane, X. Liu, J. Chen, C. Ji, E. Endler, R. Li, L. Liu *et al.*, "Lithium-ion battery fast charging: a review," *ETransportation*, vol. 1, p. 100011, 2019.

[30] X.-G. Yang, S. Ge, T. Liu, Y. Leng, and C.-Y. Wang, "A look into the voltage plateau signal for detection and quantification of lithium plating in lithium-ion cells," *Journal of Power Sources*, vol. 395, pp. 251–261, 2018.

[27] D. H. Doughty and E. P. Roth, "A general discussion of li ion battery safety," *The Electrochemical Society Interface*, vol. 21, no. 2, pp. 37–44, 2012.

[28] T. M. Bandhauer, S. Garimella, and T. F. Fuller, "A critical review of thermal issues in lithium-ion batteries," *Journal of the Electrochemical Society*, vol. 158, no. 3, pp. R1–R25, 2011.

[29] C. Rasmussen and C. Williams, *Gaussian Processes for Machine Learning*, ser. Adaptive Computation and Machine Learning. Cambridge, MA, USA: MIT Press, Jan. 2006.

[31] J. Hong, Z. Wang, F. Ma, J. Yang, X. Xu, C. Qu, J. Zhang, T. Shan, Y. Hou, and Y. Zhou, "Thermal Runaway Prognosis of Battery Systems Using the Modified Multi-Scale Entropy in Real-World Electric Vehicles," *IEEE Transactions on Transportation Electrification*, pp. 1–1, 2021.

Roya Firoozi is a postdoctoral researcher in the Department of Aeronautics and Astronautics at the Stanford University. She received her Ph.D. in Mechanical Engineering from University of California, Berkeley in 2021, and her bachelor's degree in Mechanical Engineering from University of California, Berkeley in 2014. Her current research interests are in the area of predictive control, optimization, learning and robotics.

Sara Sattarzadeh is a graduate student in the Department of Mechanical Engineering at The Pennsylvania State University. She received her bachelor's degree in electrical engineering from Shiraz University in 2011, and her master's degree in electrical engineering from Amirkabir University of Technology in 2014, Iran, Tehran. In the period of 2018-2020 she worked as a Graduate Research Assistant in University of Colorado Denver. Her current research interests include energy and transportation systems, control, estimation and diagnostics algorithms for batteries, and electric vehicles.

Satadru Dey is an assistant professor in the Department of Mechanical Engineering at The Pennsylvania State University. From August 2017 through August 2020, he was an assistant professor at University of Colorado Denver. He received his Ph.D. in Automotive Engineering from Clemson University in 2015 and Master's degree in Control Systems from Indian Institute of Technology Kharagpur, India in 2010. He was a postdoctoral researcher at University of California, Berkeley from 2015 through 2017. His technical background is in the area of controls and his research interest lies in smart cities, energy and transportation systems.